

# On hadron deformation: a model independent extraction of EMR from pion photoproduction data

L. Markou<sup>1</sup>, E. Stiliaris<sup>2</sup> and C. N.Papanicolas<sup>1,\*</sup>

<sup>1</sup> The Cyprus Institute, K. Kavafi 20, 2121 Nicosia, Cyprus

<sup>2</sup> National and Kapodistrian University of Athens, Physics Department, 15771 Athens, Greece  
April 7, 2024

## Abstract

The multipole content of pion photoproduction at the  $\Delta^+(1232)$  resonance has been extracted from a data set dominated by recent Mainz Microtron (MAMI) precision measurements. The analysis has been carried out in the Athens Model Independent Analysis Scheme (AMIAS), thus eliminating any model bias. The benchmark quantity for nucleon deformation,  $EMR = E2/M1 = E_{1+}^{3/2}/M_{1+}^{3/2}$ , was determined to be  $-2.5 \pm 0.4_{stat+syst}$ , thus reconfirming in a model independent way that the conjecture of baryon deformation is valid. The derived multipole amplitudes provide stringent constraints on QCD simulations and QCD inspired models striving to describe hadronic structure. They are in good agreement with phenomenological models which explicitly incorporate pionic degrees of freedom and with lattice QCD calculations.

**PACS.** 13.60.Rj -Baryon production 14.20.Gk -Baryon resonances ( $S = 0$ ) 24.10.Lx Monte Carlo simulations 25.20.Lj Photoproduction reactions

## 1 Introduction

The conjectured deformation of the nucleon [1, 2, 3] and of hadrons in general, has been the focus of numerous theoretical and experimental investigations for over thirty years [4, 5, 6, 7, 8, 9, 10, 11, 12, 13, 14, 15, 16, 17, 18, 19, 20] as it addresses a fundamental question in physics: the shape of the smallest particles in nature known to have size.

The anticipated deformation of hadrons is attributed to fundamental QCD processes: the color hyperfine interaction and its tensor component in particular [21, 22, 23, 24] gives rise to hadron deformation in a similar manner that nucleon-nucleon tensor interaction gives rise to the deuteron deformation. It is also recognized that equally fundamental complex chiral dynamics are at work which lead to the deformation of the nucleon's pion cloud. These same fundamental features of QCD are also responsible for many other aspects of hadron structure such as the non-vanishing neutron charge RMS radius and the magnitude of their magnetic moments.

The resulting non spherical components, predominantly D-wave admixtures, in the nucleon wavefunction allow

quadrupole excitation of the  $\Delta$  which would be absent if only S-waves were present. The ratio of electric quadrupole  $E2$  to magnetic dipole  $M1$  amplitudes (EMR) measured in the  $\gamma p \rightarrow \Delta^+(1232)$  transition serves as the accepted gauge of the magnitude of the deformation of the proton [2]. QCD simulations in lattice gauge theories and QCD inspired models yield non vanishing EMR. However both the theoretical calculations and the experimental results need to reach higher accuracy and precision to guide theoretical efforts for a better understanding of this fundamental issue.

Invariably, the experimental investigations to measure EMR utilize the transitions:

$$\gamma p \rightarrow \Delta^+(1232) \rightarrow \begin{cases} n\pi^+ \\ p\pi^0 \\ \gamma p \end{cases} \quad (1)$$

where a photon ( $\gamma$ ), real or virtual, excites a proton ( $p$ ) to a  $\Delta^+(1232)$  which de-excites with the emission of a pion ( $\pi$ ) or a gamma ray. The  $\Delta^+(1232)$  resonance ( $J = I = 3/2, \Gamma = 117 MeV$ ) [25] decays 99.4% to the  $\pi N$  channel and (0.55 – 0.65)% to the  $\gamma$  channel [25]. Its shape and width are dominated by the  $\pi N$  interaction.

As the final state of the  $\gamma N \rightarrow \pi N$  lies in the continuum, the number of possible contributing multipoles is very large, in principle infinite. Apart from the resonant multipoles, all other multipoles are termed as “background” deriving primarily from Born terms and from the tails of higher resonances [16]. Due to insufficient data [26, 27] and limitations of the analysis techniques [28] multipole analyses up to now have been able to extract only few multipoles. Higher multipoles are either set to zero (truncated analysis) or use models to account for them (model dependent analysis). This model dependence, unavoidably, leads to shifted mean values and underestimated uncertainties in the extracted multipoles and the EMR. It has been argued that in the  $\Delta(1232)$  region the model error could significantly influence the results [29, 30] making it difficult to extract multipoles with the necessary accuracy so as to provide constraints and guidance to the various theoretical models or to address the issue of nucleon deformation.

In the work presented here both limitations have been overcome: a) A rich and precise dataset has been assembled which includes the most recent pion photoproduction data to date [31, 32, 33, 34] and adequate experimental observables to allow a model independent multipole extraction and b) the Athens Model Independent Analysis Scheme (AMIAS) [35, 36] has been employed for the analysis of the data. For the first time AMIAS inherent capability to incorporate systematic error in the analysis and treat it on the same footing as statistical error has been implemented. Thus, the results presented in this work derive from the most recent and most accurate photoproduction data available, some of them used for the first time for multipole analysis [31, 32, 33, 34], employing the most complete analysis scheme currently available.

In this paper multipoles are classified using the standard  $\pi N$  notation in which a multipole is noted as  $X_{\ell\pi\pm}^I$  where  $X = E, M$  indicates its character - electric or magnetic,  $J$  its total angular momentum,  $I$  its isospin,  $\ell_\pi$  its orbital angular momentum; “+” or “-” is used to denote whether the spin ( $s=1/2$ ) is parallel or anti-parallel to the angular momentum.

## 2 The experimental database

High accuracy neutral pion photoproduction data in the  $\Delta(1232)$  region were acquired at MAMI [31, 32, 33, 34] by the A2 collaboration [37]. These data include the unpolarized differential cross section  $d\sigma_0$  [31], and the polarization-dependent differential cross sections  $\sigma T$  [32, 33, 34] and  $\sigma F$  [32, 33, 34] associated with the target asymmetry  $T$  and the beam-target asymmetry  $F$  respectively. The  $\hat{T} = \sigma T$  observable was measured with a transversely polarized target [32, 33, 34] and it features higher statistical precision and angular coverage over earlier measurements

[38]. The  $\hat{F} = \sigma F$  observable was measured for the first time using a transversely polarized target with a longitudinally polarized beam [32, 33, 34].

The  $d\sigma_0$  [31] is the most precise  $\gamma p \rightarrow p\pi^0$  cross section measured to date characterized by unprecedented statistical accuracy and extended angular coverage. It features a fine binning in  $E_\gamma$  of  $4MeV$  and covers the full pion production angle in 30 angular bins. The polarization data feature  $1.1MeV$  bins in  $E_\gamma$  and 18 evenly spaced angular bins from  $5^\circ$  to  $175^\circ$ . All aforementioned data were measured with the use of the Glasgow-Mainz photon tagging facility [39, 40, 41]. The Crystal Ball [42] and the TAPS multiphoton detector [43, 44] served as central and forward calorimeters respectively.

Fig. 1 shows the unpolarized  $d\sigma_0$  and the  $\hat{T}$  and  $\hat{F}$  polarization data; the experimental observations are in good agreement with both the MAID07 model (red solid curve) and the SAID (CM12) solution (green dashed curve). Only statistical errors are shown.

In our analysis the recent MAMI data were complemented by the older but still most precise  $\gamma p \rightarrow n\pi^+$  data of Beck *et al.* [7] for unpolarized cross section ( $d\sigma_0$ ) and beam asymmetry ( $\Sigma$ ) and the double polarization beam-target  $G$  and  $P$  asymmetries of Ahrens *et al.* [45] and Belyaev *et al.* [46]. The  $G$  asymmetry was measured using a  $4\pi$  detector system, a linearly polarized tagged photon beam, and a longitudinally polarized proton target.  $P$  was measured using linearly polarized photons and a transversely polarized proton target [46]. The  $G$  and  $P$  measurements feature only a limited number of angular measurements of low statistical precision but as it will be shown in section 4.1 they are important in restricting the derived multipole solutions. The analyzed dataset is listed in Table 1.

Table 1: The experimental data used in this work. Data in the  $\Delta(1232)$  region presented and used for the first time are indicated by a \*.

Observable	$E_\gamma (MeV)$	Ref.	datapoints
$\gamma p \rightarrow p\pi^0$			
$d\sigma_0$	337.6 - 342.0	[31]	30
$\Sigma$	335 - 345	[47]	17
$T^*$	339.0 - 340.1	[32, 33, 34]	18
$F^*$	339.0 - 340.1	[32, 33, 34]	18
$G$	326 - 354	[45]	3
$P$	335 - 365	[46]	6
$\gamma p \rightarrow n\pi^+$			
$d\sigma_0$	335 - 345	[7]	10
$\Sigma$	335 - 345	[7]	10
$T$	335 - 356	[38]	11
$G$	335 - 356	[45]	6
$P$	330 - 350	[48]	6

### 3 Methodology

The methodology employed is the implementation of the Chew, Goldberger, Low and Nambu (CGLN) theory [49] in the Athens Model Independent Analysis Scheme (AMIAS) [35, 36] for use with photoproduction data. In the case of single pion photoproduction,  $\gamma N \rightarrow N\pi$ , both initial particles and the final state nucleon have two spin states yielding a total of eight degrees of freedom [7, 16]. Due to parity conservation a total of four complex amplitudes are required to describe the reaction [7]. The four invariant amplitudes of the photoproduction process are related to the CGLN amplitudes  $(F_1, F_2, F_3, F_4)$  by a linear and invertible transformation [49, 50].

The AMIAS method is based on statistical concepts and relies heavily on Monte Carlo and simulation techniques, and it thus requires High Performance Computing as it is computationally intensive. The method identifies and determines with maximal precision parameters that are sensitive to the data by yielding their Probability Distribution Function (PDF). The AMIAS is computationally robust and numerically stable. It has been successfully applied in the analysis of data from nucleon electroproduction resonance [35, 3], lattice QCD simulations [51] and medical imaging [52].

AMIAS requires that the parameters to be extracted from the experimental data are explicitly linked via a theory or a model [35]. This requirement is fulfilled, like in the case of electroproduction ref. [35, 53], as multipoles are connected to the pion photoproduction observables via the CGLN [49] amplitudes. The multipole series of the CGLN amplitudes  $(F_i, i = 1, 4)$  takes the form [49]:

$$F_1 = \sum_{l=0}^{\infty} [(lM_{l+} + E_{l+}) P'_{l+1}(x) + ((l+1)M_{l-} + E_{l-}) P'_{l-1}(x)] \quad (2)$$

$$F_2 = \sum_{l=1}^{\infty} [(l+1)M_{l+} + lM_{l-}] P'_l(x) \quad (3)$$

$$F_3 = \sum_{l=1}^{\infty} [(E_{l+} - M_{l+}) P''_l(x) + (E_{l-} + M_{l-}) P''_{l-1}(x)] \quad (4)$$

$$F_4 = \sum_{l=2}^{\infty} [M_{l+} - E_{l+} - M_{l-} - E_{l-}] P''_{l-1}(x) \quad (5)$$

where  $x = \cos(\theta)$  is the cosine of the scattering angle. It is also assumed that in addition to unitarity the use of

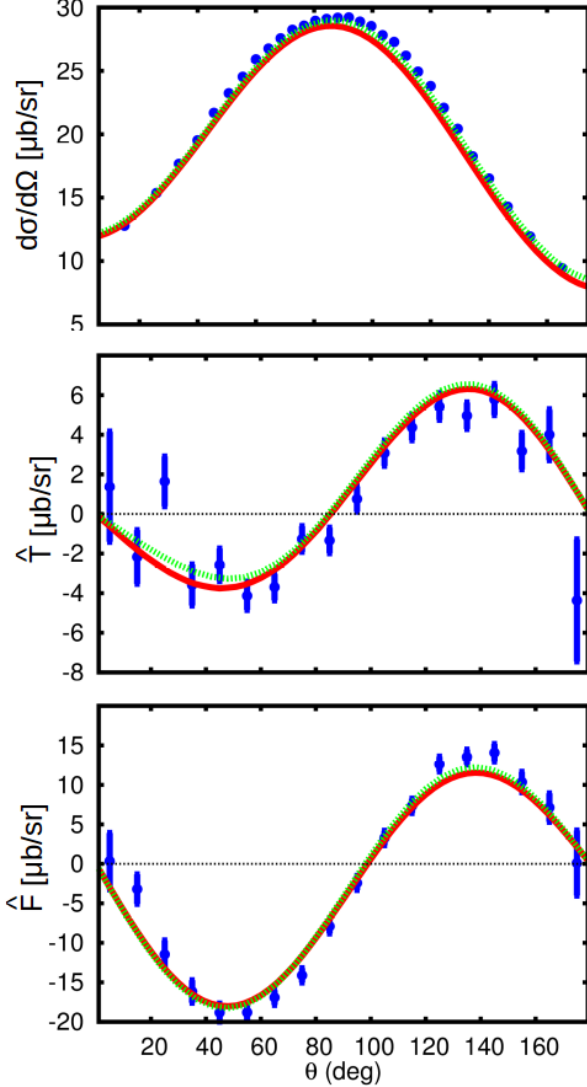


Figure 1: The high precision MAMI data used in our analysis at  $W_{cm} = 1232 MeV$ . From top to bottom are the  $\gamma p \rightarrow p\pi^0$  differential cross section [31], the polarized target  $\hat{T}$  observable [32, 33, 34] and the first ever measurement of the polarized beam-target  $\hat{F}$  observable [32, 33, 34]. The red solid and the green dashed curves are the MAID07 prediction and the SAID (CM12) solution at the same energy.

the Fermi-Watson theorem [54] applies below the two-pion threshold which in turn implies that the multipole phases in photoproduction are equal to the  $\pi N$  scattering phase shifts [55]. By fixing the multipole phases from the experimentally determined  $\pi N$  phases [35, 55] the parameters of the problem become definite isospin multipole amplitudes, namely, the  $A^{1/2}$  and  $A^{3/2}$  amplitudes [16]. These amplitudes are obtained from the reaction channel amplitudes and the relations [16]:

$$A^{1/2} = \frac{A_{p\pi^0}}{3} + \frac{\sqrt{2}A_{n\pi^+}}{3}, \quad A^{3/2} = A_{p\pi^0} - \frac{A_{n\pi^+}}{\sqrt{2}} \quad (6)$$

The Fermi-Watson theorem provides a particularly useful constraint enabling the model independent analysis as it has been shown that the number of discrete ambiguities in unconstrained truncated multipole analyses rises exponentially with the number of multipoles being fitted [56, 57]. In contrast to the practice adhered up to now where multipoles which are not fitted are either fixed through a model [13, 58] or through their Born contribution [7], we exploit the AMIAS's robustness and numerical stability to extract all multipole amplitudes to which the data exhibit any sensitivity. This feature of AMIAS is discussed in [51] and it is demonstrated in this work by extracting multipole amplitudes by gradually increasing the  $\ell_{cut}$ , where  $\ell_{cut}$  is the upper summation limit of eq. (2) - (5). All multipoles of order higher than  $\ell_{cut}$  which are not varied are fixed to their Born contribution which is calculated up to all orders [59]. We adhere to the MAID convention [16] and definitions concerning "Born terms", which thus contain s- and u-channel nucleon terms,  $\rho$  and  $\omega$  exchange in the t-channel, and pion pole contributions [16] which are significant in the charged pion channel. Above a given multipole order the derived PDFs remain unchanged as more amplitudes are allowed to vary, indicating that convergence has been reached and maximal information has been extracted from the data. As a convergence criterion for the PDFs we use a T-statistics test [60, 61] and demand that the derived  $\ell_{cut}$  multipole PDFs differ no more than  $\sim 2\%$  from the  $\ell_{cut} + 1$  PDFs. The minimum  $\chi^2$  value generated during each  $\ell_{cut}$  analysis also reaches an asymptotic value as the analyses are driven towards convergence. This means that allowing higher waves to vary would not contribute to the  $\chi^2$  value of the problem, as the data are completely insensitive to them. A flowchart of the AMIAS implementation for multipole extraction from photoproduction data is illustrated in Fig. 2.

Multipole extraction from photoproduction data is an inverse problem posing a highly complex [8] and correlated parameter space [28, 62]. Capturing all these correlations is essential for dealing with the numerous and individually weakly contributing background amplitudes and producing precise results. Model dependent methods freeze

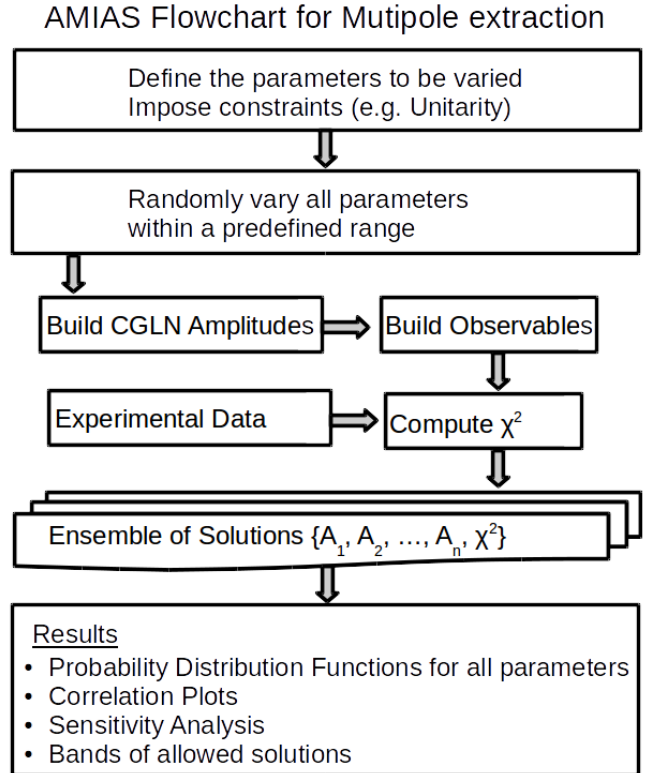


Figure 2: AMIAS flowchart for multipole extraction. The term parameters includes multipoles, nuisance parameters and kinematical variables.

“insensitive” multipoles thus excluding any possibility of determining them and more importantly removing their influence on the dominant amplitudes, through correlations, which can be substantial. Such an approach introduces uncontrolled model error which may both shift the extracted values for the dominant amplitudes and underestimate the corresponding uncertainty. Implementing the AMIAS postulate [35, 36], that “every physically accepted solution is a solution to the problem with a finite probability of representing reality”, through unbiased MC sampling of the entire parameter space, all possible correlations between the parameters and up to all orders are captured and embedded in the AMIAS ensemble of solutions. The full accounting of correlations is one of the main features of AMIAS that minimizes the model error.

### 3.1 Treatment of systematic errors

Modern accelerators and detection instrumentation have allowed significant improvements in the quality of pion-photoproduction data, often yielding results characterized by statistical errors smaller than the estimated systematic uncertainties [31]. This requires a more complex and sophisticated treatment of systematic effects in multipole extraction analyses. In previous analyses, this was either ignored or accommodated by simply adding in quadrature the systematic and statistical uncertainties. In the  $\Delta(1232)$  region, the dominant  $M_{1+}^{3/2}$  amplitude is very sensitive to systematic errors of multiplicative nature while the small resonant  $E_{1+}^{3/2}$  amplitude is in addition sensitive to angular precision [7].

To account for possible sources of systematic uncertainty whose leading effect on the data is either of multiplicative or of additive nature (pedestal) we have introduced nuisance parameters for the unpolarized cross section data and the model:

$$d\sigma_0^i \rightarrow \alpha_i \cdot d\sigma_0^i + c_i \quad (7)$$

where the coefficients (nuisance parameters)  $\alpha_i$  and  $c_i$  are allowed to vary in a restricted range according to the magnitude of the reported estimated systematic uncertainty [7, 31]. The index- $i$  is used to distinguish between the  $p\pi^0$  and the  $n\pi^+$  differential cross sections. An uncertainty in determining the center-of-mass (CM) pion angle of up to  $2^\circ$  is reported for the Crystal Ball/Taps system [63] and it was taken into account by allowing the CM angle that freedom during the variation (AMIAS Monte Carlo) procedure. The uncertainty in incident photon energy  $E_{\gamma,lab}$  and center-of-mass energy  $W_{cm}$  [31, 41] was found to induce a negligible effect to the data at the resonance region.

### 3.2 Validation of the applied methodology

The AMIAS methodology for the case of electro- and photoproduction has been extensively studied and validated through the analysis of pseudodata [35, 36, 53]; also in several other reactions and cases [51, 52].

The case of resonance photoproduction presented here was extensively studied; an indicative example of multipole amplitude extraction employing the aforementioned methodology using the pseudodata of [64] is shown here. The analyzed pseudo-dataset contains high precision simulation data for the differential cross section ( $d\sigma_0$ ), the beam ( $\Sigma$ ), the target ( $T$ ) and the beam-target ( $F$ ) asymmetries for the  $\gamma p \rightarrow p\pi^0$  and the  $\gamma p \rightarrow n\pi^+$  reactions. The data were generated by randomizing the MAID07 [65] model as input at the CM energy  $W = 1232.23 MeV$ . They contain eighteen even spaced angular measurements for each observable in the dynamical region  $\theta_{cm} \in [5^\circ : 175^\circ]$ , where  $\theta_{cm}$  is the angle between the incoming photon and the outgoing pion in the CM frame [64].

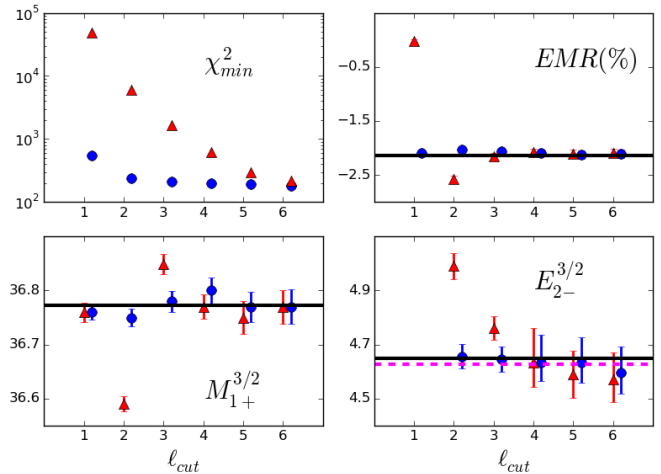


Figure 3: From left to right and top to bottom: The minimum  $\chi^2$  value generated, the extracted  $EMR(\%)$ ,  $M_{1+}^{3/2}$  and  $E_{2-}^{3/2}$  as functions of the angular momentum number  $\ell$ . Red triangles: Truncated analysis. Blue dots: Multipoles which are not varied are fixed by Born terms. The generator values ( $EMR_{MAID07} = -2.14\%$ ). The Born contribution to a multipole is marked by a dashed magenta line.

By applying the methodology of Sec. 3 we extracted multipole amplitudes of up to  $\ell_{cut} = 6$  where convergence was reached. The  $\chi_{min}^2$  found in the AMIAS ensemble of solutions as the  $\ell_{cut}$  increased is illustrated in Fig. 3-a where the color-coding red triangles was used for the truncated analysis (multipoles which are not varied are set to zero) while the blue circles were used for the analysis dur-

ing which amplitudes that were not varied were fixed to their Born value. The derived values for  $EMR(\%)$  and two selected amplitudes,  $M_{1+}^{3/2}$  and  $E_{2-}^{3/2}$  are also illustrated from  $\ell_{cut} = 1$  up to convergence. The results shown depict the mean for the derived multipole PDF with an confidence level corresponding to a  $\pm 34\%$  probability. The black horizontal line is the generator input while the magenta line shows the Born contribution to the multipole. All extracted multipoles show a similar behavior; they are in statistical agreement with the generator input and converge by  $\ell_{cut} = 6$ . It is worth noting that the results of the truncated analysis are characterized by large fluctuations as the imposed  $\ell_{cut}$  is increased. This indicates that higher waves are needed to reliably extract lower multipoles.

## 4 Results

By applying the methodology presented in Section 3 to the experimental data of Table 1 we extracted values for all multipole amplitudes which show sensitivity to the data. Multipoles of up to  $\ell_{cut} = 5$  were varied before convergence was reached. In Figs 4 and 5 the PDFs of some selected  $\ell \leq 2$  multipoles from the AMIAS model independent analysis are compared to the  $\ell = 1$  and  $\ell = 2$  model dependent (MD) analysis and the Bonn - Gatchina [66, 67], the MAID07 [65] and the SAID-PR15 [68, 69] solutions. MD analyses recognize the influence of non resonant multipoles of order higher than those allowed by the imposed truncation  $\ell_{cut}$ , typically  $\ell_{cut} = 1$  and  $\ell_{cut} = 2$ , on the derived resonant terms; instead of ignoring them they give them values derived from phenomenological models. In the results shown in Figs 4 and 5 the higher than  $\ell_{cut}$  background terms were fixed to the MAID07 values. In general, we observe good agreement between the derived mean values between the AMIAS and the MD analyses. We note significant differences in the derived uncertainties between the AMIAS and the MD analyses. The AMIAS extracted values agree with those of the phenomenological models which fall within one or two standard deviations from the experimentally determined values. The sole exception is the MAID07 value for the multipole amplitudes  $E_{0+}^{1/2}$  and  $E_{0+}^{3/2}$  where a larger than  $3\sigma$  discrepancy is observed. The extracted amplitudes with  $\ell \geq 3$  are not shown in the figures but they are in good statistical agreement with model predictions which treat these background amplitudes as primarily deriving from Born terms.

The multipole PDFs derived from the AMIAS analysis were fitted by asymmetric gaussians and numerical results were extracted. Table 2 lists the mean value and 68% confidence (CL) for each of the sensitive multipoles. As sensitive were considered all multipole amplitudes with relative uncertainty less than 50%. The quoted uncertainties of the

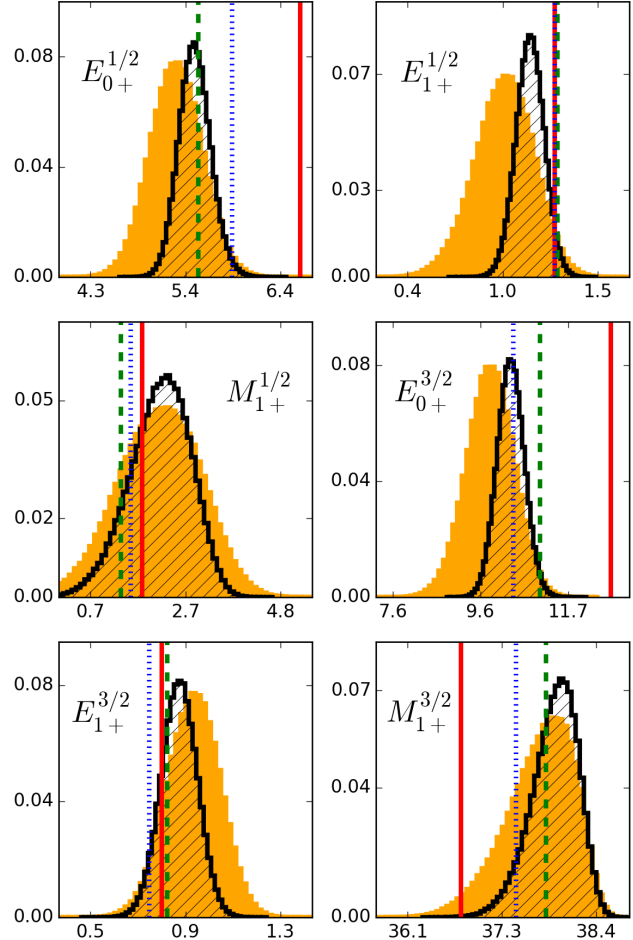


Figure 4: PDFs of  $\ell \leq 1$  extracted multipole amplitudes. The AMIAS solution is colored in orange while the Model Dependent (MD)  $\ell_{cut} = 1$  solution in the hatched histogram. The vertical lines show model predictions: MAID07 (red-continuous), SAID-PR15 (green-dashed), and Bonn-Gatchina-2014-02 (blue-dotted).

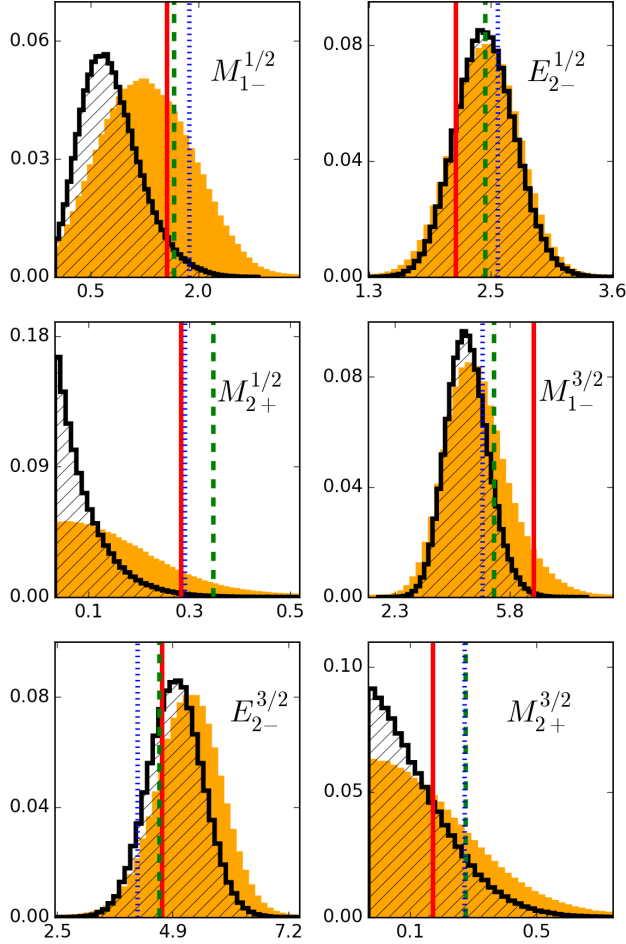


Figure 5: PDFs of  $\ell \leq 2$  extracted multipole amplitudes. Same conventions as in Fig. 4 are used.

Table 2: AMIAS Extracted values and 68% confidence level (CL) for all the multipoles exhibiting sensitivity to the data of Table 1. The results are presented with decreasing accuracy, which is the measured relative uncertainty (RU). Only multipoles with relative uncertainty  $< 50\%$  are listed. The MAID07 [65], SAID-(PR15) [31, 69] and Bonn-Gatchina [66, 67] model values are tabulated for comparison. In boldface are the predictions which lie outside the 95% CL. Multipoles are given in units of  $10^{-3}/m_\pi$ .

Multipole	MAID07	SAID	BG	AMIAS	RU(%)
$M_{1+}^{3/2}$	36.7	37.8	37.3	$37.7 \pm_{0.5}^{0.3}$	0.9
$E_{0+}^{3/2}$	<b>12.7</b>	<b>11.0</b>	10.4	$10.0 \pm_{0.6}^{0.5}$	5.5
$E_{0+}^{1/2}$	<b>6.6</b>	5.5	<b>5.9</b>	$5.3 \pm_{0.3}^{0.3}$	5.7
$E_{2-}^{3/2}$	4.6	4.6	<b>4.2</b>	$5.5 \pm_{0.6}^{0.6}$	10.9
$E_{2-}^{1/2}$	2.11	2.6	2.5	$2.57 \pm_{0.30}^{0.27}$	11.1
$E_{1+}^{3/2}$	0.79	0.81	0.73	$0.94 \pm_{0.13}^{0.11}$	12.8
$E_{1+}^{1/2}$	1.27	1.28	1.26	$1.07 \pm_{0.16}^{0.13}$	13.6
$M_{1-}^{3/2}$	6.6	5.4	5.0	$4.5 \pm_{0.6}^{1.0}$	17.8
$M_{2-}^{1/2}$	0.55	0.60	0.62	$0.88 \pm_{0.20}^{0.14}$	19.3
$M_{1+}^{1/2}$	1.8	1.4	1.6	$3.0 \pm_{0.9}^{0.6}$	25.0
$E_{2+}^{1/2}$	0.36	0.39	0.38	$0.28 \pm_{0.08}^{0.07}$	26.8
$E_{3-}^{1/2}$	0.48	0.46	0.47	$0.42 \pm_{0.12}^{0.12}$	28.6
$E_{4+}^{3/2}$	0.08	<b>0.07</b>	<b>0.07</b>	$0.18 \pm_{0.05}^{0.06}$	30.6
$E_{3+}^{3/2}$	0.19	0.19	0.19	$0.28 \pm_{0.10}^{0.08}$	32.1
$E_{3-}^{3/2}$	0.61	0.56	0.64	$0.65 \pm_{0.21}^{0.25}$	35.4
$E_{4-}^{3/2}$	0.20	0.19	0.19	$0.40 \pm_{0.14}^{0.15}$	36.3
$E_{3+}^{1/2}$	0.13	0.12	0.13	$0.11 \pm_{0.04}^{0.04}$	36.4
$M_{3-}^{3/2}$	0.15	0.14	0.15	$0.38 \pm_{0.14}^{0.16}$	39.5
$M_{2-}^{3/2}$	0.54	0.42	0.59	$0.63 \pm_{0.23}^{0.31}$	42.9
$E_{2+}^{3/2}$	0.55	0.65	0.56	$0.39 \pm_{0.13}^{0.23}$	46.2
$M_{3-}^{1/2}$	0.11	0.12	0.10	$0.15 \pm_{0.06}^{0.08}$	46.7

extracted multipoles include both statistical and systematic errors and contain no model error. The relative uncertainties, are also tabulated. The values of the MAID07, SAID-PR15 and BG-2014-02 models are also shown in the same table for comparison. It is important to highlight the fact that the AMIAS method exhibits numerical stability even when non-sensitive multipoles are allowed to vary.

The visualization of the correlations between any two extracted parameters is accomplished in a two-dimensional scatter plot in which the AMIAS ensemble of solutions are projected on the plane defined by the parameter values and color coded according to the  $\chi^2$  value of each solution. The correlations between the two resonant amplitudes  $E_{1+}^{3/2}$  and  $M_{1+}^{3/2}$  and the resonant and some background amplitudes are shown in Fig. 6. The resonant amplitudes do not exhibit significant correlation among them whereas there are some mild correlations between the resonant  $E_{1+}^{3/2}$  and background amplitudes. Some background amplitudes, *e.g.*  $M_{1+}^{1/2}$  and  $M_{1-}^{1/2}$  illustrated in Fig. 7, exhibit moderate correlations when derived from the full dataset of Table 1 but are highly correlated when derived from the “reduced dataset” which lacks the information of the double polarization  $P$  and  $G$  observables, thus highlighting the importance of double polarization observables.

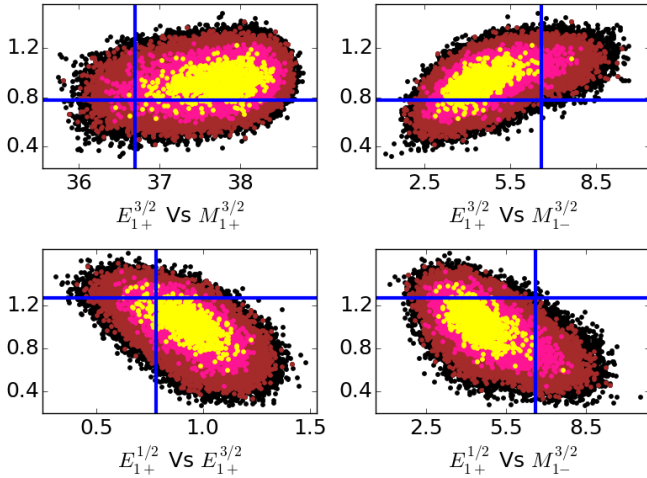


Figure 6: Correlation plots between the resonant and selected background amplitudes. The blue lines indicate the MAID07 model prediction. Color coded as:  $\chi^2 \leq 1.1 \cdot \chi_{min}^2$  (yellow),  $\chi^2 \leq 1.2 \cdot \chi_{min}^2$  (pink),  $\chi^2 \leq 1.3 \cdot \chi_{min}^2$  (brown), no  $\chi^2$  cut (black).

#### 4.1 Bands of allowed solutions

The AMIAS ensemble of solutions, can be used to select any subset of solutions which represent “reality” within a given CL. This is achieved by building the histogram of

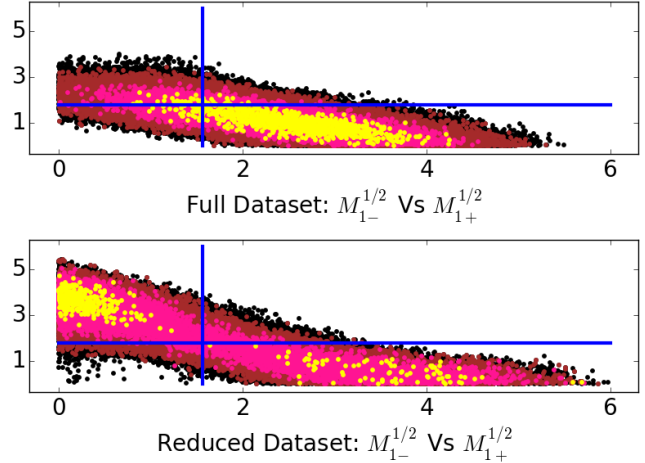


Figure 7: Correlation plots between the two background amplitudes  $M_{1+}^{1/2}$  and  $M_{1-}^{1/2}$ . Top: Extracted from the full database of Table 1. Bottom: Extracted from the reduced dataset. The blue cross indicates the MAID07 model prediction. Color coded according to the scheme of fig. 6.

the generated  $\chi^2$ 's forming subsequently from it the corresponding PDF and integrating it to the desired CL. In comparison to other approximate methods, *e.g.* the  $UP$  parameter method [70] of MINUIT [71] the AMIAS method is exact. The investigation of the properties of the acceptable solutions can reveal valuable information on the detailed interpretation of the derived results or the potential value of missing measurements.

Using this technique we explore the value of the double polarization observables. We selected the solutions from the AMIAS ensemble leading to a 68% CL to describing the data. These solutions include values for each of the single and double Beam-Target polarization observables which are illustrated as bands in Fig. 8. The yellow more restricted bands correspond to solutions allowed by the full dataset (Table 1) while the blue, more relaxed, bands correspond to solutions to a restricted data set which the double polarization observables  $G$  and  $P$  have been removed. This comparison demonstrates the importance of double polarization observables in restricting the multipole solutions. It also indicates the desirability of obtaining data in the very forward and backward angles. Such bands, are also particularly valuable in assessing the value of observables which need to be measured and the desired accuracy in order to achieve more precise results.

## 5 Extracted EMR

The derived value of EMR(%),  $-2.5 \pm 0.4_{stat+sys}$ , is free of model error, the first time this has been achieved. It



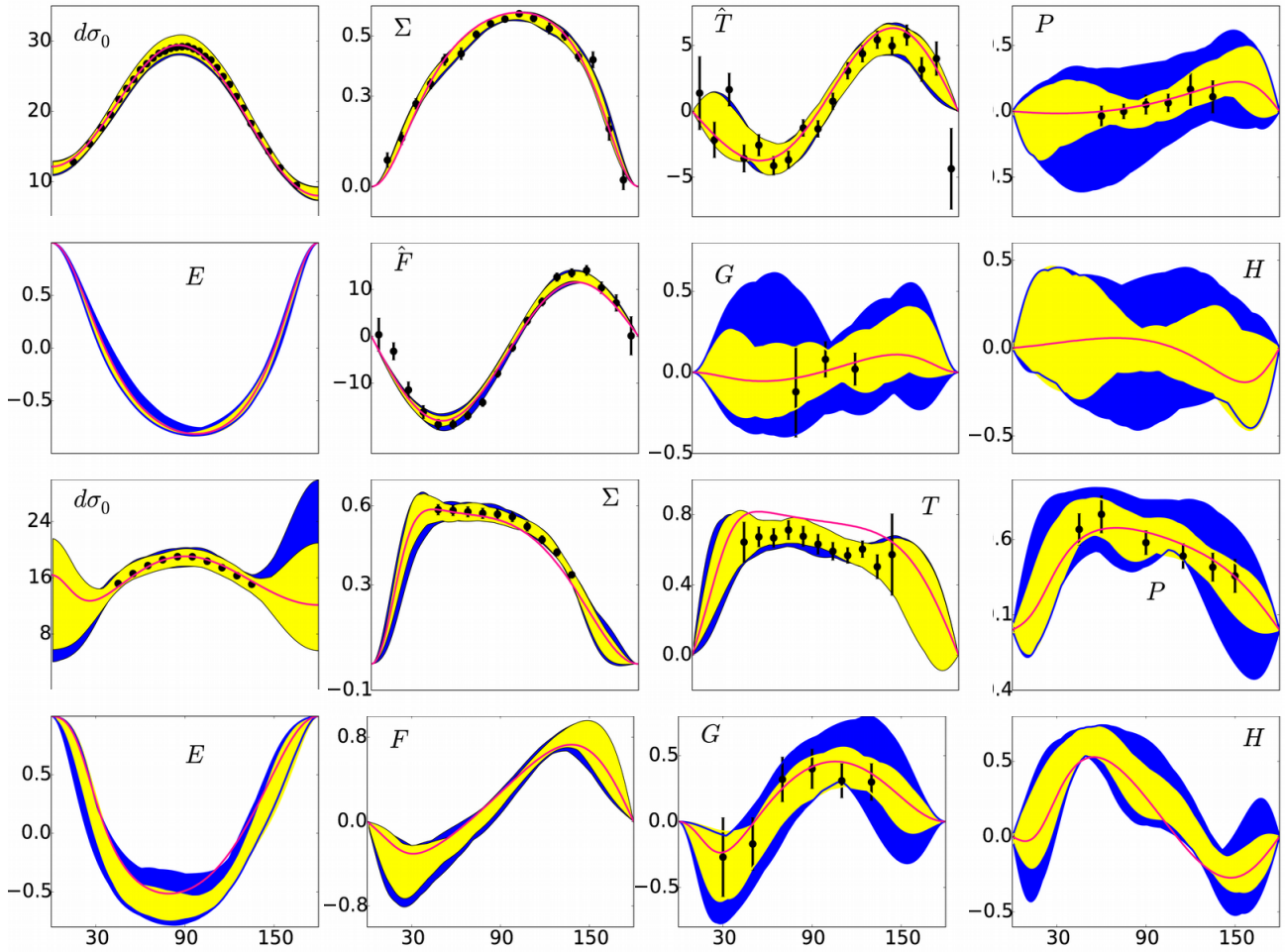


Figure 8: Bands of allowed solutions with a 68% confidence level and a full  $\theta_{cm}$  angular coverage for the four single and four beam-target pion photoproduction observables. The top two rows concern the  $\gamma p \rightarrow p\pi^0$  channel while the two bottom the  $n\pi^+$  channel. Blue bands: the reduced dataset is used. Yellow bands: the full dataset is used. The pink curve is the MAID07 model prediction. Cross sections are given in units of  $\mu b/sr$ .

is in good agreement with earlier reports [7, 8, 12]. Special care was taken to account for any systematic errors as described in Section 3.1, for which their effect on the derived EMR value was estimated to be  $\pm 0.1\%$ . The magnitude of uncertainty due to systematics was estimated by comparing the PDF of EMR when systematic errors were accounted for, and when ignored.

Although a nearly complete dataset was used, which utilizes the most precise measurements to date, the derived uncertainty is comparable to analyses of older and less precise data. This is due to the fact that model dependent analyses in which background multipoles are fixed also freeze the correlations to other multipoles [29] thus reducing the propagated uncertainty. This is manifested in the PDFs shown in Figs. 4 and 5 where it is evident that the Model Independent AMIAS results (PDFs) are noticeably broader than those resulting from the Model Dependent analysis. Model independent analysis of the “benchmark dataset” [28] has shown that the traditional ansatz [29] of employing several different models and attributing the spread in the solutions as model error [30] although not precise it adequately captures the magnitude of the effect.

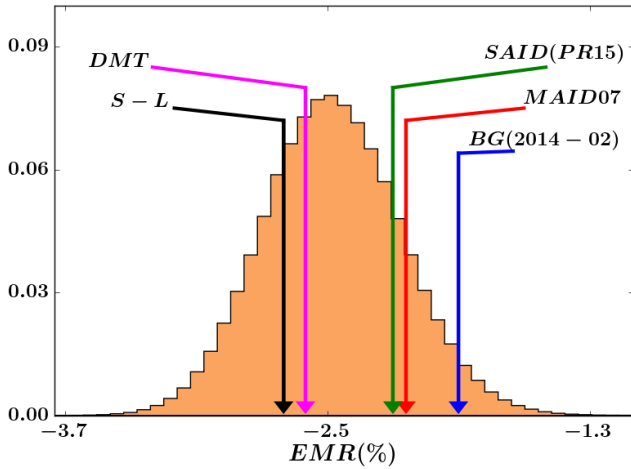


Figure 9: PDF of the derived EMR(%) from the full dataset of Table 1. Both statistical and systematic errors were considered. The vertical lines represent model predictions.

In Table 3 we present the EMR values of various analyses and models of the last 20 years and make a distinction to the kind of quoted error, statistical, model, and systematic. Excluding the BRAG result [30] which quotes only a model uncertainty and not a statistical error, all other analyses report a statistical+model error combined which is comparable or larger than the  $\pm 0.4\%$  value determined in this work. Of the listed analyses, only in the works of references [7, 8, 12] the analyzed data allowed for full multipole isospin decomposition and in each of them a different

approach was used to fix the background. References [7] and [12] fix all  $\ell \geq 2$  by following the Born approximation. The tabulated EMR value from [7] is from a single energy fit to experimental data while in [12] EMR was determined using the so-called W-dependent approach which explains the very small statistical errors. Ahrens [12] parameterize all multipoles which are not resonant by a simple second-order polynomial function with a smooth energy dependence. These assumptions contribute to a model error which is estimated by the authors to be 0.3%. In [8]  $(\gamma, \gamma)$  multipoles are also considered, while the  $(\pi, \gamma)$  multipole series was truncated at  $\ell = 3$ . The general good agreement between the EMR of this work, the earlier reported values, the latest lattice QCD calculation [20] and the model predictions shows that the phenomenological models and the model assumptions used up to now are valid. Based on this analysis we understand that the observed robustness of the extracted EMR can be attributed to the development of successful phenomenological models but also to the fact that the resonant amplitudes exhibit little correlation with the background amplitudes.

Table 3: Selected EMR(%) values from various experiments, analyses and models reported in the last 20 years.

Experiment/Analysis	EMR(%)
<b>This work</b>	<b><math>-2.5 \pm 0.4_{stat+syst}</math></b> <sup>(1)</sup>
PDG [25]	$-2.5 \pm 0.5$ <sup>(2)</sup>
Beck '97 [4]	$-2.5 \pm 0.2_{stat} \pm 0.2_{model}$
Blanpied '97 [5]	$-3.0 \pm 0.3_{stat+syst} \pm 0.2_{model}$
BRAG [30]	$-2.37 \pm 0.27$ <sup>(3)</sup>
Beck '01 [7]	$-2.5 \pm 0.1_{stat} \pm 0.2_{model}$
Blanpied '01 [8]	$-3.07 \pm 0.26_{stat+syst} \pm 0.24_{model}$
Ahrens '04 [12]	$-2.74 \pm 0.03_{stat} \pm 0.3_{model}$ <sup>(4)</sup>
Kotulla '07 [15]	$-2.4 \pm 0.16_{stat} \pm 0.24_{model}$
<b>Models</b>	<b>EMR(%)</b>
Fernandez-Ramirez [72]	$-3.9 \pm 1.1$
Pascalutsa - Tjon [73]	$-2.6 \pm 0.6$
SAID (PR15) [68]	$-2.1$
Bonn-Gatchina [66]	$-1.9$
MAID07 [65]	$-2.2$
DMT [74]	$-2.6$
Sato-Lee (S-L) [17]	$-2.7$
Lattice QCD [20]	$-3.1 \pm 2.1_{stat}$ <sup>(5)</sup>

1. Model Independent Analysis.
2. PDG result is an average of several independent reports.
3. Quoted uncertainty is purely model and is the spread of several analyses over the same data.
4. Quotes BRAG result as model error.
5.  $Q^2 = 0.154(GeV^2)$ ,  $m_\pi = 297 MeV$ .

## 6 Conclusions

A dataset of pion photoproduction data which allows for full isospin decomposition was analyzed at a single energy right on top of the  $\Delta^+(1232)$  resonance. The data contain the most recent and most precise measurements to date. For the analysis, the AMIAS method was employed which allowed the extraction of all multipole amplitudes to which the data exhibited any sensitivity. Our analysis revealed strong correlations between background amplitudes and some mild correlations between background amplitudes and the resonant  $E_{1+}^{3/2}$  amplitude. Since the  $E_{1+}^{3/2}$ 's determined uncertainty dominates the EMR, capturing all correlations between the parameters was an important issue in our analysis which was fully addressed. The  $EMR(\%) = -(2.5 \pm 0.4_{stat+syst})$  reported here is for the first time free of any model error. Its good compatibility with phenomenological models and earlier analyses confirms the validity of the model assumptions behind the analysis methods used up to now. The model independent results of this work corroborate earlier reports, *e.g.* [13], which highlight the central role the pion cloud plays in nucleon structure [29] as a consequence of the spontaneous chiral symmetry breaking. The derived results, of unprecedented accuracy reconfirm and validate the conjecture of nucleon deformation attributing it mostly to pion nucleon dynamical interplay.

## Acknowledgements

The authors would like to thank the A2-collaboration for making the recent MAMI measurements available for analysis. We are very much indebted to Reinhard Beck, Michael Ostrick (with support from the Deutsche Forschungsgemeinschaft DFG-CRC1044), Sergey Prakhov and Yannick Wunderlich for enlightening discussions concerning data analysis and experimental and model uncertainties along with Vladimir Pascalutsa, Lothar Tiator and Marc Vanderhaeghen for exhaustive discussions on theoretical aspects of nucleon dynamics and nucleon resonance photoexcitation. This work, part of L. Markou Doctoral Dissertation, was supported by the Graduate School of The Cyprus Institute.

## References

- [1] Sheldon L. Glashow. The unmellisonant quark. *Physica A*, 96(1-2):27–30, 1979.
- [2] C. N. Papanicolas and A. M. Bernstein. *Shapes of hadrons*. AIP conference proceedings. 2007.
- [3] C. Alexandrou, C. N. Papanicolas, and M. Vanderhaeghen. Colloquium. *Rev. Mod. Phys.*, 84:1231–1251, Sep 2012.
- [4] R. Beck, H. P. Krahn, J. Ahrens, H. J. Arends, G. Audit, A. Braghieri, N. d’Hose, S. J. Hall, V. Isbert, J. D. Kellie, I. J. D. MacGregor, P. Pedroni, T. Pinelli, G. Tamas, Th. Walcher, and S. Wartenberg. Measurement of the  $E2/M1$  Ratio in the  $\gamma n \rightarrow \Delta(1232)$  Transition using the reaction  $p(\gamma, p)\pi^0$  and  $p(\gamma, \pi^+)n$ . *Phys. Rev. Lett.*, 78:606–609, Jan 1997.
- [5] G. Blanpied, M. Blecher, A. Caracappa, C. Djalali, G. Giordano, K. Hicks, S. Hoblit, M. Khandaker, O. C. Kistner, A. Kuczewski, et al.  $N \rightarrow \Delta$  Transition from Simultaneous Measurements of  $p(\gamma, \pi)$  and  $p(\gamma, \gamma)$ . *Phys. Rev. Lett.*, 79(22):4337, 1997.
- [6] Valery Victor Frolov, GS Adams, Abdellah Ahmidouch, CS Armstrong, Ketevi Assamagan, Steven Avery, O’Keith Baker, Peter Bosted, Volker Burkert, Roger Carlini, et al. Electroproduction of the  $\Delta(1232)$  resonance at high momentum transfer. *Phys. Rev. Lett.*, 82(1):45, 1999.
- [7] R. Beck, HP Krahn, J. Ahrens, JRM Annand, HJ Arends, G Audit, A Braghieri, N dHose, D Drechsel, O Hanstein, et al. Determination of the  $e\ 2/m\ 1$  ratio in the  $\gamma\ n\ \delta\ (1232)$  transition from a simultaneous measurement of  $p(\gamma, p)\ \pi\ 0$  and  $p(\gamma, \pi^+)\ n$ . *Phys. Rev. C*, 61(3):035204, 2000.
- [8] G. Blanpied, M. Blecher, A. Caracappa, R. Deinger, C. Djalali, G. Giordano, K. Hicks, S. Hoblit, M. Khandaker, O. C. Kistner, et al.  $N \rightarrow \Delta$  transition and proton polarizabilities from measurements of  $p(\gamma, \gamma)$ ,  $p(\gamma, \pi^0)p$ , and  $p(\gamma, \pi^+)n$ . *Phys. Rev. C*, 64(2):025203, 2001.
- [9] C. Mertz, C. E. Vellidis, R. Alarcon, D. H. Barkhuff, A. M. Bernstein, W. Bertozzi, V. Burkert, J. Chen, J. R. Comfort, G. Dodson, S. Dolfini, K. Dow, M. Farkhondeh, J. M. Finn, S. Gilad, R. W. Gothe, X. Jiang, K. Joo, N. I. Kaloskakis, A. Karabarbounis, J. J. Kelly, S. Kowalski, C. Kunz, R. W. Lourie, J. I. McIntyre, B. D. Milbrath, R. Miskimen, J. H. Mitchell, C. N. Papanicolas, C. F. Perdrisat, A. J. Sarty, J. Shaw, S.-B. Soong, D. Tieger, C. Tschalær, W. Turchinets, P. E. Ulmer, S. Van Verst, G. A. Warren, L. B. Weinstein, S. Williamson, R. J. Woo, and A. Young. Search for quadrupole strength in the electroexcitation of the  $\Delta^+(1232)$ . *Phys. Rev. Lett.*, 86:2963–2966, Apr 2001.
- [10] P. Bartsch, D. Baumann, J. Bermuth, R. Böhm, K. Bohinc, Damir Bosnar, M. Ding, M. Distler, D. Drechsel

- sel, D Elsner, et al. Measurement of the Beam-Helicity Asymmetry in the  $p(e, ep)\pi^0$  Reaction at the Energy of the  $\Delta(1232)$  Resonance. *Phys. Rev. Lett.*, 88(14):142001, 2002.
- [11] K. Joo, L. C. Smith, V. D. Burkert, R. Minehart, I. G. Aznauryan, L. Elouadrhiri, S. Stepanyan, G. S. Adams, M. J. Amarian, E. Anciant, M. Anghinolfi, D. S. Armstrong, B. Asavapibhop, G. Audit, T. Auger, H. Avakian, S. Barrow, H. Bagdasaryan, M. Battaglieri, K. Beard, M. Bektasoglu, W. Bertozzi, N. Bianchi, A. S. Biselli, S. Boiarinov, B. E. Bonner, W. K. Brooks, J. R. Calarco, G. P. Capitani, D. S. Carman, B. Carnahan, P. L. Cole, A. Coleman, D. Cords, P. Corvisiero, D. Crabb, H. Crannell, J. Cummings, E. De Sanctis, R. De Vita, P. V. Degtyarenko, R. A. Demirchyan, H. Denizli, L. C. Dennis, A. Deppman, K. V. Dharmawardane, K. S. Dhuga, C. Djalali, G. E. Dodge, D. Doughty, P. Dragovitsch, M. Dugger, S. Dytman, M. Eckhause, Y. V. Efremenko, H. Egiyan, K. S. Egiyan, L. Farhi, R. J. Feuerbach, J. Ficenecc, K. Fissum, T. A. Forest, H. Funsten, M. Gai, V. B. Gavrilov, S. Gilad, G. P. Gilfoyle, K. L. Giovanetti, P. Girard, K. A. Griffioen, M. Guidal, M. Guillo, V. Gyurjyan, D. Hancock, J. Hardie, D. Heddle, J. Heisenberg, F. W. Hersman, K. Hicks, R. S. Hicks, M. Holtrop, C. E. Hyde-Wright, M. M. Ito, D. Jenkins, J. H. Kelley, M. Khandaker, K. Y. Kim, W. Kim, A. Klein, F. J. Klein, M. Klusman, M. Kossov, Y. Kuang, S. E. Kuhn, J. M. Laget, D. Lawrence, A. Longhi, K. Loukachine, M. Lucas, R. W. Major, J. J. Manak, C. Marchand, S. K. Matthews, S. McAleer, J. W. C. McNabb, B. A. Mecking, M. D. Mestayer, C. A. Meyer, M. Mirazita, R. Miskimen, V. Muccifora, J. Mueller, G. S. Mutchler, J. Napolitano, G. Niculescu, B. Nizyoporuk, R. A. Niyazov, M. S. Ohandjanyan, A. Opper, Y. Patois, G. A. Peterson, S. Philips, N. Pivnyuk, D. Pocanic, O. Pogorelko, E. Polli, B. M. Preedom, J. W. Price, L. M. Qin, B. A. Raue, A. R. Reolon, G. Riccardi, G. Ricco, M. Ripani, B. G. Ritchie, F. Ronchetti, P. Rossi, D. Rowntree, P. D. Rubin, C. W. Salgado, M. Sanzone, V. Sapunenko, M. Sargsyan, R. A. Schumacher, Y. G. Sharabian, J. Shaw, S. M. Shuvalov, A. Skabelin, E. S. Smith, T. Smith, D. I. Sober, M. Spraker, P. Stoler, M. Taiuti, S. Taylor, D. Tedeschi, R. Thompson, L. Todor, T. Y. Tung, M. F. Vineyard, A. Vlassov, H. Weller, L. B. Weinstein, R. Welsh, D. P. Weygand, S. Whisnant, M. Witkowski, E. Wolin, A. Yegneswaran, J. Yun, Z. Zhou, and J. Zhao.  $q^2$  dependence of quadrupole strength in the  $\gamma^*p \rightarrow \Delta^+(1232) \rightarrow p\pi^0$  transition. *Phys. Rev. Lett.*, 88:122001, Mar 2002.
- [12] J Ahrens, S Altieri, JRM Annand, C Anton, HJ Arends, K Aulenbacher, R Beck, C Bradtke, A Braghieri, Natalie Degrande, et al. Helicity dependence of the... channels and multipole analysis in the... region. *Eur. Phys. J. A*, 21(2), 2004.
- [13] NF Sparveris, R Alarcon, AM Bernstein, W Bertozzi, T Botto, P Bourgeois, J Calarco, F Casagrande, MO Distler, K Dow, et al. Investigation of the conjectured nucleon deformation at low momentum transfer. *Phys. Rev. Lett.*, 94(2):022003, 2005.
- [14] R. Beck. Experiments with photons at MAMI. *Eur. Phys. J. A*, 28(1):173–183, 2006.
- [15] Martin Kotulla. Real Photon Experiments:  $N \rightarrow \Delta$  and  $\mu_\Delta$ . In *AIP Conference Proceedings*, volume 904, pages 203–212. AIP, 2007.
- [16] D Dreschsel and Lothar Tiator. Threshold pion photoproduction on nucleons. *J. Phys. G: Nucl. Part. Phys.*, 18(3):449, 1992.
- [17] T. Sato and T.-S. H. Lee. Dynamical study of the  $\Delta$  excitation in  $N(e, e'\pi)$  reactions. *Phys. Rev. C*, 63:055201, Mar 2001.
- [18] SS Kamalov, Guan-Yeu Chen, Shin Nan Yang, D Drechsel, and L Tiator.  $\pi^0$  Photo- and electroproduction at threshold within a dynamical model. *Phys. Lett. B*, 522(1):27–36, 2001.
- [19] IG Aznauryan. Multipole amplitudes of pion photoproduction on nucleons up to  $2\text{GeV}$  using dispersion relations and the unitary isobar model. *Phys. Rev. C*, 67(1):015209, 2003.
- [20] C Alexandrou, G Koutsou, JW Negele, Y Proestos, and A Tsapalis. Nucleon to  $\delta$  transition form factors with  $n_f = 2+1$  domain wall fermions. *Phys. Rev. D*, 83(1):014501, 2011.
- [21] N Isgur. N. isgur, g. karl, and r. koniuk, *phys. rev. d* 25, 2394 (1982). *Phys. Rev. D*, 25:2394, 1982.
- [22] Simon Capstick and Gabriel Karl.  $\frac{E_{1+}}{M_{1+}}$ . *Phys. Rev. D*, 41:2767–2775, May 1990.
- [23] Gilberto Ramalho, MT Pena, and Franz Gross. D-state effects in the electromagnetic  $N - \Delta$  transition. *Phys. Rev. D*, 78(11):114017, 2008.
- [24] Vladimir Pascalutsa, Marc Vanderhaeghen, and Shin Nan Yang. Electromagnetic excitation of the  $\Delta(1232)$ -resonance. *Phys. Rep.*, 437(5):125–232, 2007.

- [25] C. Patrignani et al. Review of Particle Physics. *Chin. Phys.*, C40(10):100001, 2016.
- [26] Yannick Wunderlich. Complete experiments in meson photoproduction. In *Int. J. Mod. Phys.: Conference Series*, volume 40, page 1660068. World Scientific, 2016.
- [27] A M Sandorfi, S Hoblit, H Kamano, and T-S H Lee. Determining pseudoscalar meson photoproduction amplitudes from complete experiments. *J. Phys. G: Nucl. Part. Phys.*, 38(5):053001, 2011.
- [28] L. Markou, C. N. Papanicolas, and E. Stiliaris. AMIAS Analysis of the Benchmark data. To be published.
- [29] A. M. Bernstein and C. N. Papanicolas. Overview: The shape of hadrons. In *AIP Conference Proceedings*, volume 904, pages 1–22. AIP, 2007.
- [30] RA Arndt, I Aznauryan, RM Davidson, D Drechsel, O Hanstein, SS Kamalov, AS Omelaenko, I Strakovsky, L Tiator, RL Workman, et al. Multipole analysis of a benchmark data set for pion photoproduction. In *NSTAR 2001*, volume 1, pages 467–492, 2001.
- [31] P. Adlarson et al. [A2 Collaboration]. Measurement of  $\pi^0$  photoproduction on the proton at MAMI C. *Phys. Rev. C*, 92(2):024617, 2015.
- [32] S. Schumann, B.P. Otte et al. [A2 Collaboration]. Threshold  $\pi^0$  photoproduction on transverse polarised protons at MAMI. *Phys. Lett. B*, 750:252–258, 2015.
- [33] B.P. Otte. PhD thesis, University Mainz, 2015.
- [34] J. Annand et al. [A2 Collaboration]. T and f asymmetries in  $\pi^0$  photoproduction on the proton. *Phys. Rev. C*, 93(5):055209, 2016.
- [35] E. Stiliaris and C. N. Papanicolas. Multipole extraction: A novel, model independent method. In *AIP Conference Proceedings*, volume 904, pages 257–268. AIP, 2007.
- [36] C. N. Papanicolas and E. Stiliaris. A novel method of data analysis for hadronic physics. *arXiv preprint arXiv:1205.6505*, 2012.
- [37] A2 Homepage Mainz. <https://wwa2.kph.uni-mainz.de/>.
- [38] H Dutz, D Krämer, B Zucht, KH Althoff, G Anton, J Arends, W Beulertz, A Bock, M Breuer, R Gehring, et al. Photoproduction of positive pions from polarized protons. *Nucl. Phys. A*, 601(3):319–332, 1996.
- [39] I Anthony, JD Kellie, SJ Hall, GJ Miller, and J Ahrens. Design of a tagged photon spectrometer for use with the Mainz 840 MeV Microtron. *Nucl. Instrum. Methods Phys. Res., Sect. A*, 301(2):230–240, 1991.
- [40] SJ Hall, GJ Miller, R Beck, and P Jennewein. A focal plane system for the 855 MeV tagged photon spectrometer at MAMI-B. *Nucl. Instrum. Methods Phys. Res., Sect. A*, 368(3):698–708, 1996.
- [41] JC McGeorge, JD Kellie, JRM Annand, J Ahrens, I Anthony, A Clarkson, DJ Hamilton, PS Lumsden, EF McNicoll, RO Owens, et al. Upgrade of the glasgow photon tagging spectrometer for Mainz MAMI-C. *Eur. Phys. J. A*, 37(1):129–137, 2008.
- [42] A Starostin, BMK Nefkens, E Berger, M Clajus, A Marušić, S McDonald, N Phaisangittsakul, S Prakhov, JW Price, M Pulver, et al. Measurement of  $K^-p \rightarrow \eta\Lambda$  near threshold. *Phys. Rev. C*, 64(5):055205, 2001.
- [43] Annette R Gabler, W Doering, M Fuchs, B Krusche, V Metag, R Novotny, M Röbig-Landau, H Ströher, V Tries, C Molenaar, et al. Response of TAPS to monochromatic photons with energies between 45 and 790 MeV. *Nucl. Instrum. Methods Phys. Res., Sect. A*, 346(1-2):168–176, 1994.
- [44] Rainer Novotny. The  $BaF_2$  photon spectrometer TAPS. *IEEE Trans. Nucl. Sci.*, 38(2):379–385, 1991.
- [45] J. Ahrens, S. Altieri, J. R. M. Annand, H. J. Arends, and R. Beck. Measurement of the G asymmetry for the  $\gamma p \rightarrow n\pi$  channels in the  $\Delta(1232)$  resonance region. *Eur. Phys. J. A*, 26(1):135–140, 2005.
- [46] AA Belyaev, VA Get'man, VG Gorbenko, VA Gushchin, A Ya Derkach, Yu V Zhebrovsky, IM Karnaukhov, L Ya Kolesnikov, AA Lukhanin, AS Omelayenko, et al. Experimental studies of the  $\Sigma$ , T, P polarization parameters and the  $\gamma p \rightarrow p\pi^0$  reaction multipole analysis in the first resonance region. *Nucl. Phys. B*, 213(2):201–222, 1983.
- [47] R Leukel. PhD thesis, University Mainz, 2001.
- [48] VA Get'man, VG Gorbenko, A Ya Derkach, Yu V Zhebrovskij, IM Karnaukhov, L Ya Kolesnikov, AA Lukhanin, AL Rubashkin, PV Sorokin, EA Sporov, et al. Positive pion production from polarized protons by linearly polarized photons in the energy range 280 – 420 MeV. *Nucl. Phys. B*, 188(3):397–413, 1981.
- [49] G. Chew, M. Goldberger, F. Low and Y. Nambu. Relativistic dispersion relation approach to photomeson production. *Phys. Rev.*, 106(6):1345, 1957.

- [50] O. Hanstein, D. Drechsel, and L. Tiator. Multipole analysis of pion photoproduction based on fixed  $t$  dispersion relations and unitarity. *Nucl. Phys. A*, 632(4):561 – 606, 1998.
- [51] C. Alexandrou, T. Leontiou, C. N. Papanicolas, and E. Stiliaris. Novel analysis method for excited states in lattice qcd: The nucleon case. *Phys. Rev. D*, 91(1):014506, 2015.
- [52] C. N. Papanicolas, L. Koutsantonis, and E. Stiliaris. A Novel Analysis Method for Emission Tomography. To be published.
- [53] L. Markou. *Doctoral Thesis*. PhD thesis, The Cyprus Institute, 2018. (In preparation).
- [54] Kenneth M. Watson. Some general relations between the photoproduction and scattering of  $\pi$  mesons. *Phys. Rev.*, 95:228–236, Jul 1954.
- [55] RL Workman, RA Arndt, WJ Briscoe, MW Paris, and II Strakovsky. Parameterization dependence of  $t$ -matrix poles and eigenphases from a fit to  $\pi n$  elastic scattering data. *Phys. Rev. C*, 86(3):035202, 2012.
- [56] A Omelaenko. Ambiguities of the multipole analysis of neutral-pion photoproduction from nucleons. *Sov. J. Nucl. Phys.(Engl. Transl.);(United States)*, 34(3), 1981.
- [57] Y Wunderlich, R Beck, and L Tiator. The complete-experiment problem of photoproduction of pseudoscalar mesons in a truncated partial-wave analysis. *Physical Review C*, 89(5):055203, 2014.
- [58] RM Davidson. Model dependence of  $E2/M1$ . In *NSTAR 2001*, pages 203–206. World Scientific, 2001.
- [59] Lothar Tiator. private communication, 2016.
- [60] R Barlow. *Statistics: A Guide to the Use of Statistical Methods in the Physical Sciences*. 1993.
- [61] Frank C Porter. Testing consistency of two histograms. *arXiv preprint arXiv:0804.0380*, 2008.
- [62] César Fernández-Ramírez. The unexpected role of D waves in low-energy neutral pion photoproduction. *arXiv preprint arXiv:0912.4158*, 2009.
- [63] Christina Collicott. PhD thesis, University Mainz, 2015.
- [64] R.L. Workman, M.W. Paris, W.J. Briscoe, L. Tiator, S. Schumann, M. Ostrick, and S.S. Kamalov. Model dependence of single-energy fits to pion photoproduction data. *Eur. Phys. J. A*, 47(11), 2011.
- [65] D. Drechsel, S. S. Kamalov, and L. Tiator. Unitary Isobar Model - MAID2007. *Eur. Phys. J.*, A34:69–97, 2007.
- [66] Bonn-Gatchina Partial Wave Analysis. <https://pwa.hiskp.uni-bonn.de/>.
- [67] E. Gutz et al. High statistics study of the reaction  $\gamma p \rightarrow p\pi^0\eta$ . *Eur. Phys. J.*, A50:74, 2014.
- [68] INS Data Analysis Center. <http://gwdac.phys.gwu.edu/>.
- [69] Ron Workman. private communication, 2017.
- [70] Multiparameter Errors in Minuit - UP values. <http://www.dnp.fmph.uniba.sk/cernlib/asdoc/minuit/node33.html>. Accessed: 2017-07-28.
- [71] Fred James et al. Minuit. *Function Minimization and Error Analysis, Version*, 94, 1994.
- [72] C Fernández-Ramírez, E Moya de Guerra, and JM Udías. Hints on the quadrupole deformation of the  $\Delta(1232)$ . *Phys. Rev. C*, 73(4):042201, 2006.
- [73] Vladimir Pascalutsa and John A Tjon. Pion photoproduction on nucleons in a covariant hadron-exchange model. *Phys. Rev. C*, 70(3):035209, 2004.
- [74] Sabit S Kamalov, Shin Nan Yang, Dieter Drechsel, Olaf Hanstein, and Lothar Tiator.  $\gamma^*n \rightarrow \Delta$  transition form-factors: A new analysis of the JLab data on  $p(e, e'p)\pi^0$  at  $Q^2 = 2.8(\text{GeV}/c)^2$  and  $4.0(\text{GeV}/c)^2$ . *Phys. Rev. C*, 64(3):032201, 2001.